Supplementary Information

Agarose-biofunctionalized, dual-electrospun heteronanofiber mats: Toward metal-ion chelating battery separator membranes

Ju-Myung Kim, Chanhoon Kim, Seungmin Yoo, Jeong-Hoon Kim, Jung-Hwan Kim, Jun-Muk Lim, Soojin Park, and Sang-Young Lee**

Experimental Section

Structural design and fabrication of dual-electrospun heteronanofiber mat (= AHM separator)

To fabricate the AHM separator, two different polymer solutions were respectively prepared. Agarose and PAA were mixed in DMF at 90 °C for 12 h, where the composition ratio of agarose/PAA was 50/50 (w/w). At the same time, 10 wt% PAN solution (solvent = DMF) was prepared. Both the agarose/PAA solution and the PAN one were simultaneously dual-electrospun via different nozzles at room temperature/30 RH%. The detailed electrospinning conditions were 7.5 kV with a feed rate of 10 μL min^{-1} (for agarose/PAA solution) and 8.5 kV with a feed rate of 10 μL min^{-1} (for PAN solution). The dual-electrospun (agarose/PAA)/PAN nanofiber mat was collected on a stainless steel plate positioned at a distance of 9 cm from the electrospinning nozzles. Subsequently, the dual-electrospun (agarose/PAA)/PAN heteronanofiber mat was subjected to thermal condensation (150 ^{o}C/2 h in a vacuum oven) and then roll-pressed at room temperature, leading to the AHM Separator (average thickness ~ 25 μm). A commercial PE separator (thickness = 20 μm, Tonen) was chosen as a control sample.

Structural/physicochemical characterization of AHM separator

The porous structure of the AHM separator was analyzed with FE-SEM (S-4800, Hitachi), EDS (JSM 6400, JEOL) and Gurley densometer (4110N, Gurley). The intermolecular hydrogen bonding between agarose and PAA was examined using FT-IR spectrometer (670-IR, Agilent). The tensile properties of the separators were measured using a universal testing machine (AGS-100NX, SHIMADZU). The electrolyte wettability of the separators was quantitatively estimated by measuring the electrolyte immersion-height. The thermal shrinkage of the separators was determined by measuring their area-based dimensional change after exposure to 150 ^{o}C/0.5 h. To quantitatively estimate the Mn^{2+} chelation ability of separators, manganese perchlorate solution (10 mM $Mn(ClO_4)_2$-containing 1.3 M $LiPF_6$ in EC/PC = 1/1 v/v) was prepared. After being soaked in the solution for 2 h at room temperature, the separators were washed with pristine EC/PC solvents (containing no $LiPF_6$ salts) and then the amount of the captured Mn^{2+} ions was analyzed by ICP-MS (ELAN DRC-II, Perkin Elmer). The interaction between Mn^{2+} ions and agarose was examined using ^{13}C NMR (400-MR DD2, Agilent).

Application of AHM separator to lithium-ion batteries

The electrochemical stability window of the AHM separator was investigated using a linear sweep voltammetry experiment performed on a working electrode of stainless-steel and a counter/reference electrode of lithium-metal at a scan rate of 1.0 mV s^{-1}. For the OCV drop measurement, the cell was pre-cycled twice at a charge/discharge current density of 0.1 C, and then fully charged at a current density of 0.2 C to 100 % charge state. Finally, the OCV drop of the fully charged cell was monitored as a function of elapsed time. The ion conductivity of the AHM separator was examined by an AC impedance analysis (VSP classic, Bio-Logic) over a frequency range of 10^{-2} - 10^{6} Hz. A unit cell (2032-type coin) was assembled by sandwiching a separator between LMO cathode (LMO/carbon black/PVdF binder = 92/3/5 w/w/w) and Li metal anode, and then activated by being filled with the liquid electrolyte (1 M $LiPF_6$ in EC/DEC = 1/1 v/v). The cell performance was investigated using a cycle tester (PNE Solution) at various

charge/discharge conditions. The structural change of electrode surface and seaparators after the cycling test was analyzed using XPS (ThermoFisher) with focused monochromatized Al Kα radiation and also ICP-MS measurement.

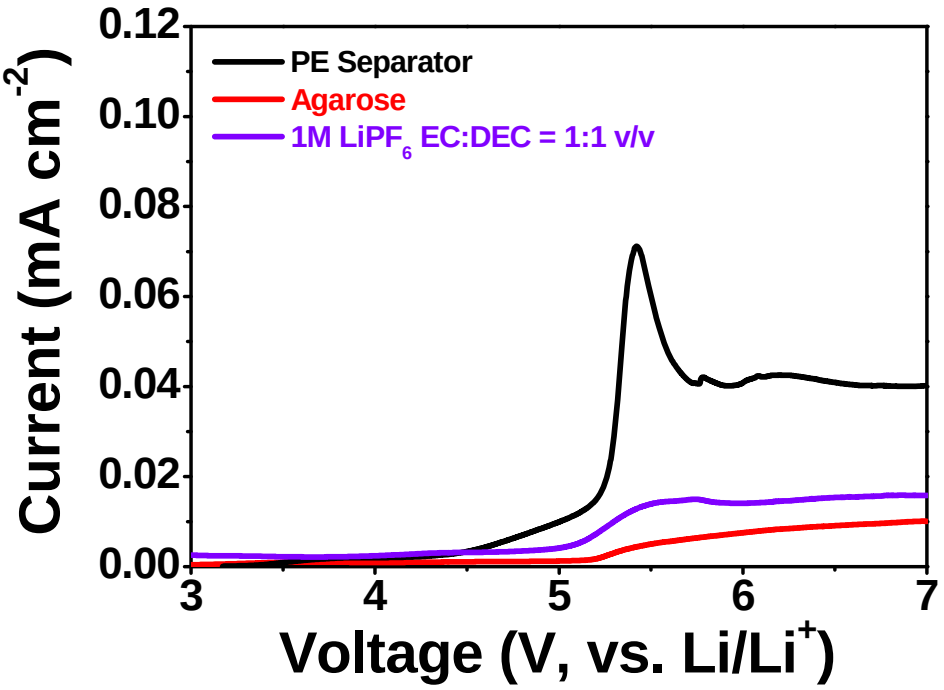

Fig. S1. Comparison in electrochemical stability between agarose film and PE Separator, where a linear sweep voltammetry experiment was performed on a working electrode of stainless steel and a counter and reference electrode of lithium-metal at a scan rate of 1 mV s^{-1}.

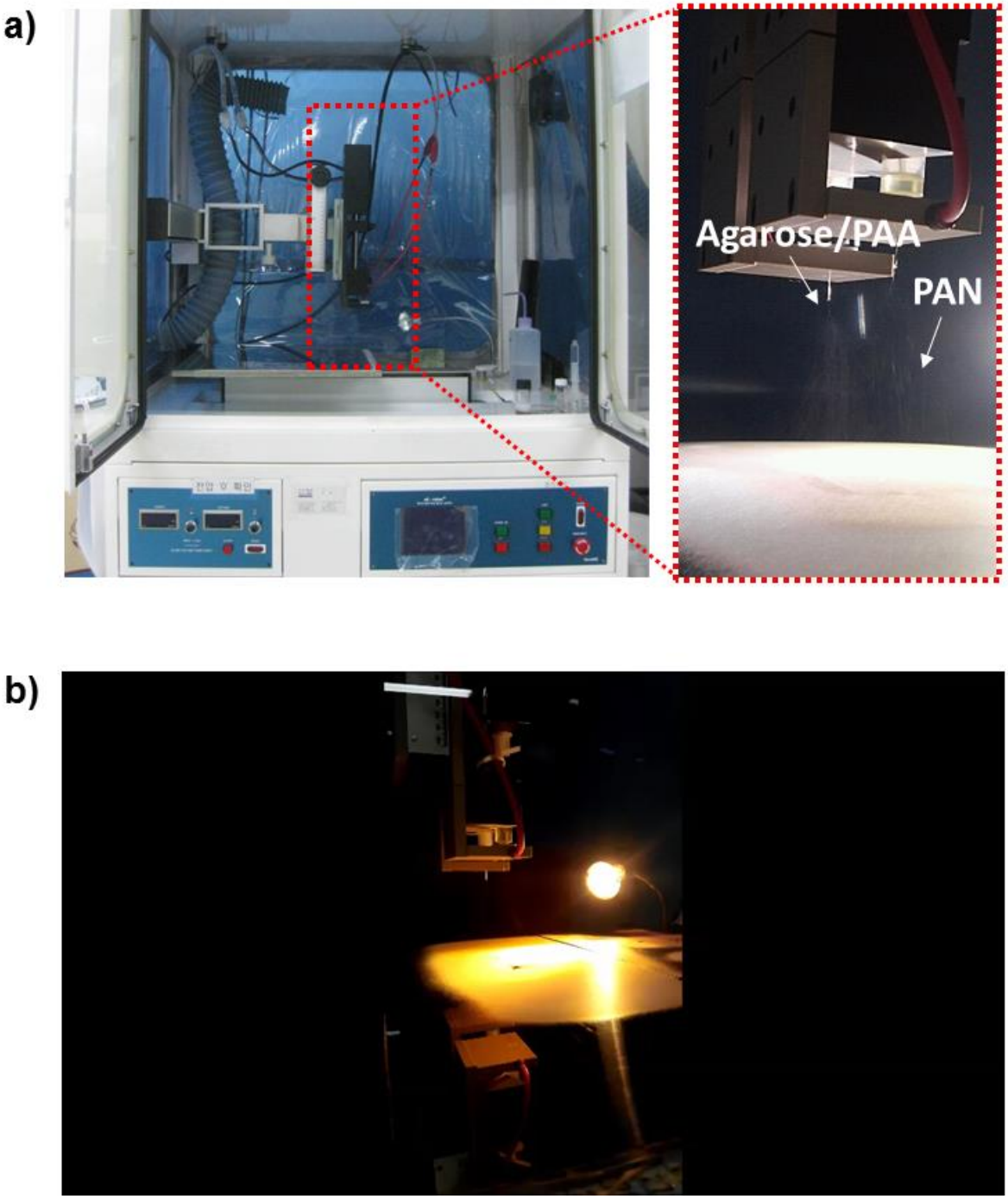

Fig. S2. Experimental operation of the dual electrospinning process used for AHM separator: (a) photographs; (b) video clip.

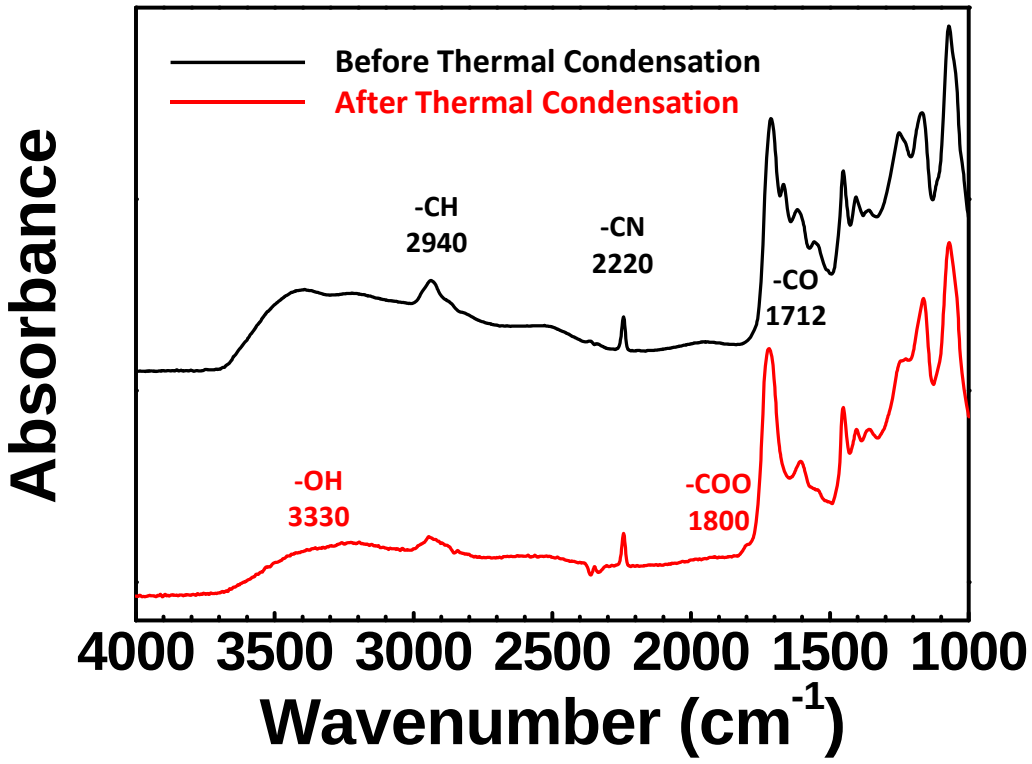

Fig. S3. FT-IR spectra showing the variation in the characteristic peaks assigned to the hydroxyl groups of agarose in the agarose/PAA nanofiber mat, before/after being subjected to thermal condensation (150 ^{o}C/2 h in a vacuum oven).

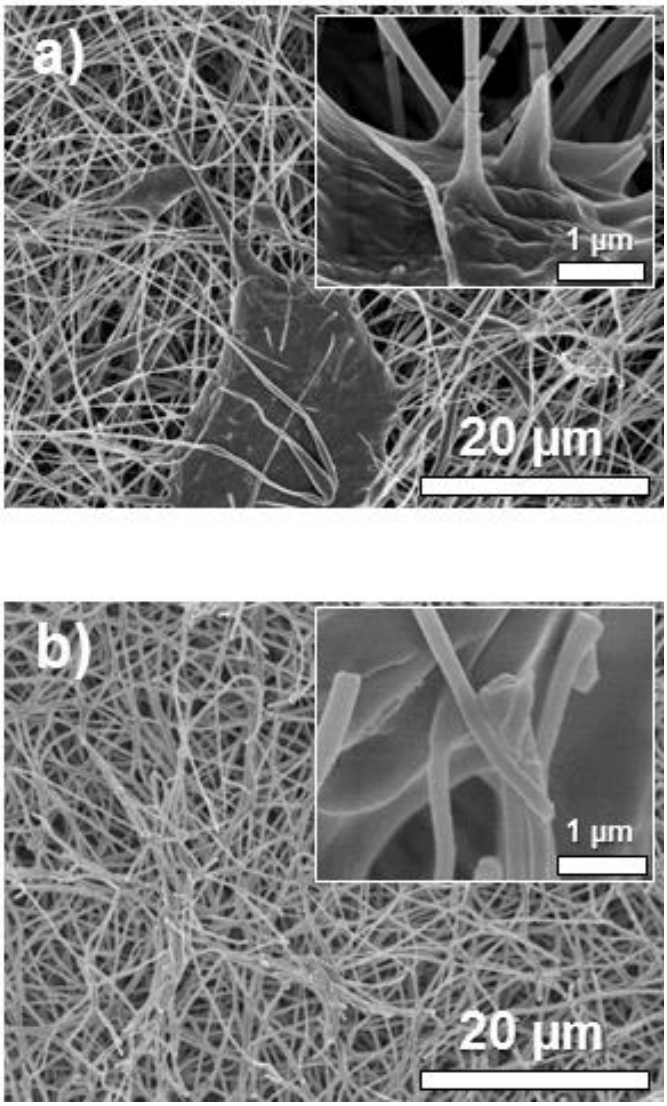

Fig. S4. Effect of agarose/PAA composition ratio on the porous structure evolution of agarose/PAA electrospun nanofiber mat: (a) agarose/PAA = 70/30 (w/w); (b) agarose/PAA = 30/70 (w/w).

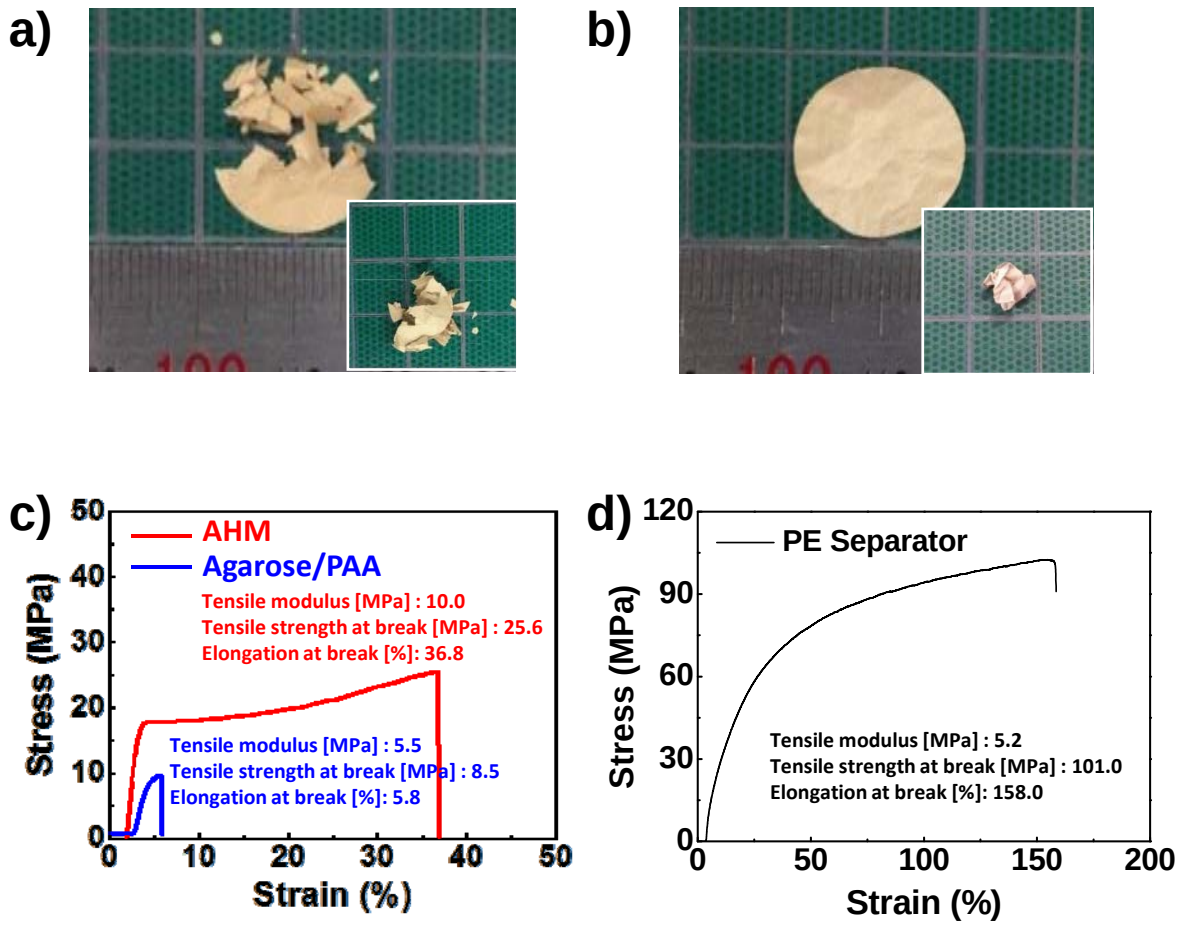

Fig. S5. Comparison in dimensional tolerance upon mechanical deformation (= wrinkling): (a) agarose/PAA nanofiber mat (wrinkled → unwrinkled); (b) (agarose/PAA)/PAN AHM separator (wrinkled → unwrinkled), wherein inset images show the wrinkled state of each separator. Stress-strain curves of: (c) agarose/PAA nanofiber mat and (agarose/PAA)/PAN AHM separator (measured at a strain rate of 10 mm min^{-1}); (d) PE separator.

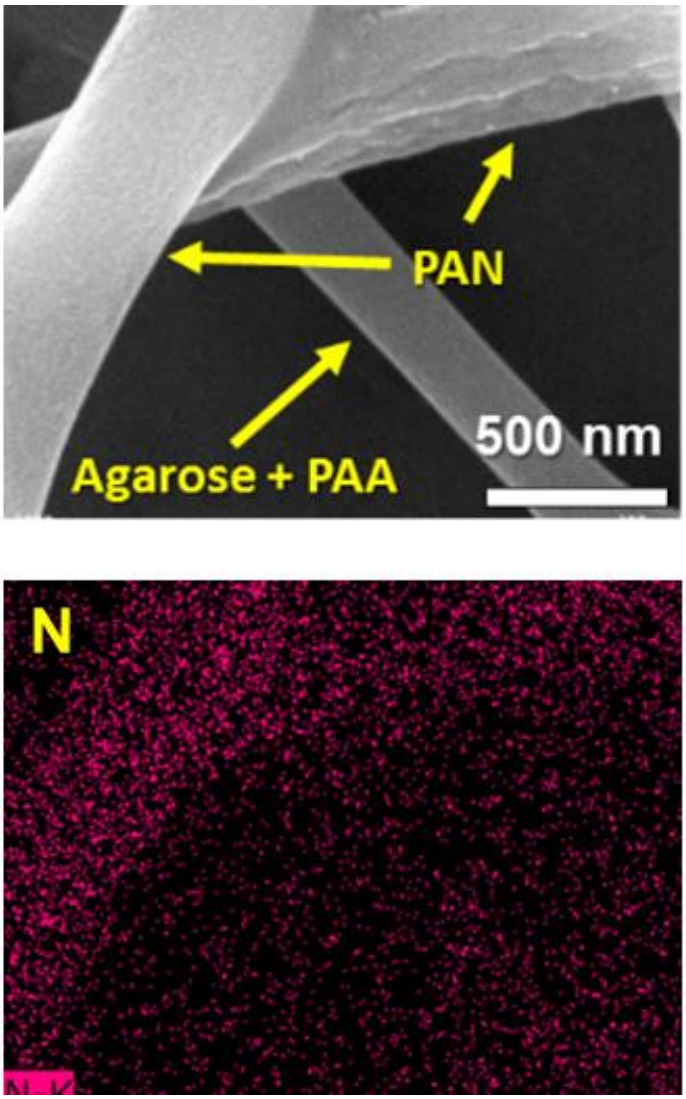

Fig. S6. Structural analysis of (agarose/PAA)/PAN AHM separator: (a) SEM image; (b) EDS image (with a particular focus on N element).

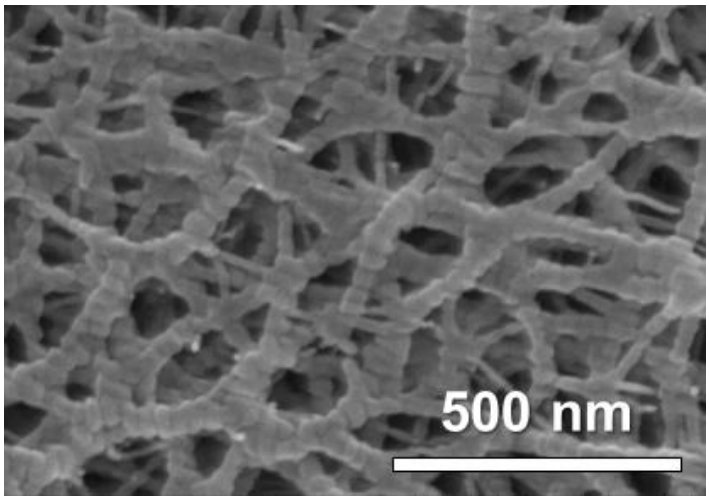

Fig. S7. SEM image (surface view) of PE separator.

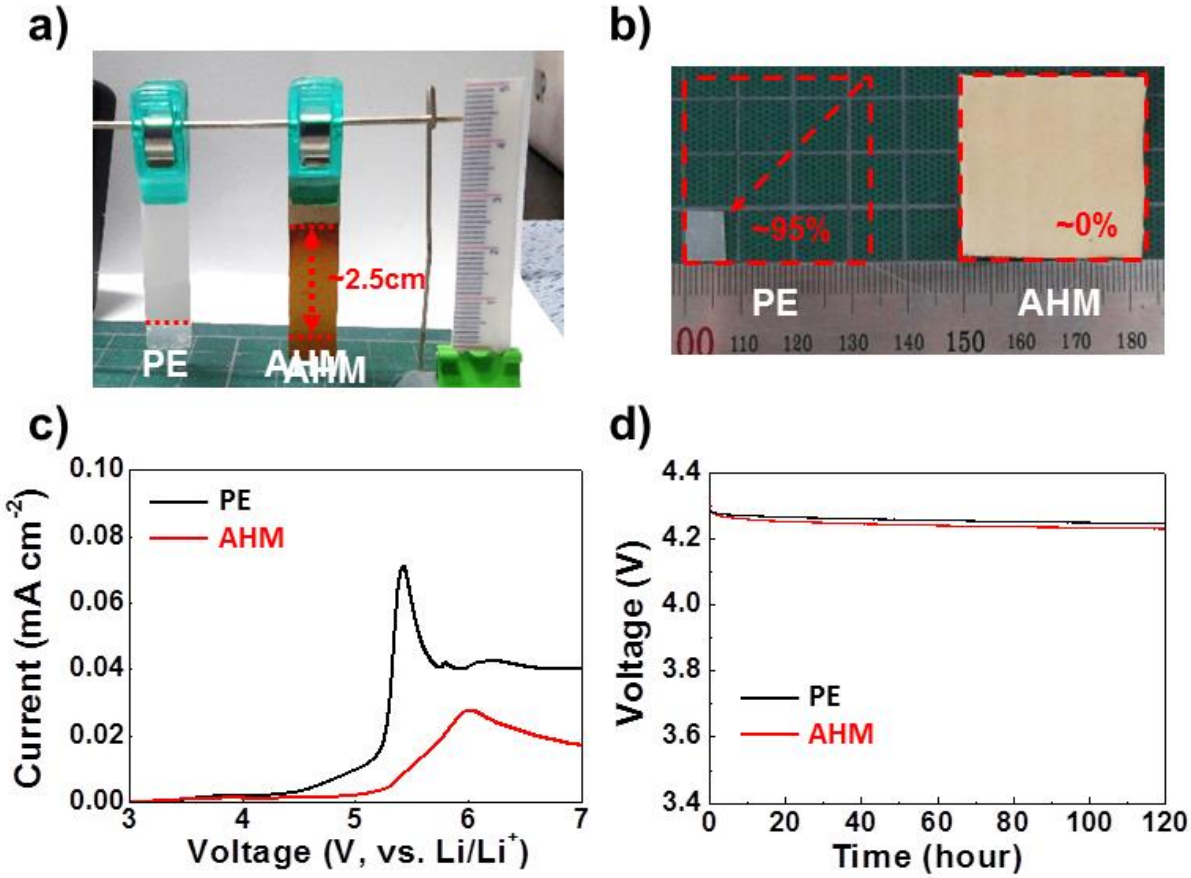

Fig. S8. Comparision in major membrane properties between AHM separator and PE separator: (a) electrolyte wettability (determined by electrolyte-immersion height); (b) thermal shrinkage after exposure to 150 ^{o}C/0.5 h; (c) linear sweep voltammograms; (d) OCV profiles of cells, where the cells were charged to 4.3 V at constant current density of 0.2 C and their voltage drop was measured as a function of the elapsed time.

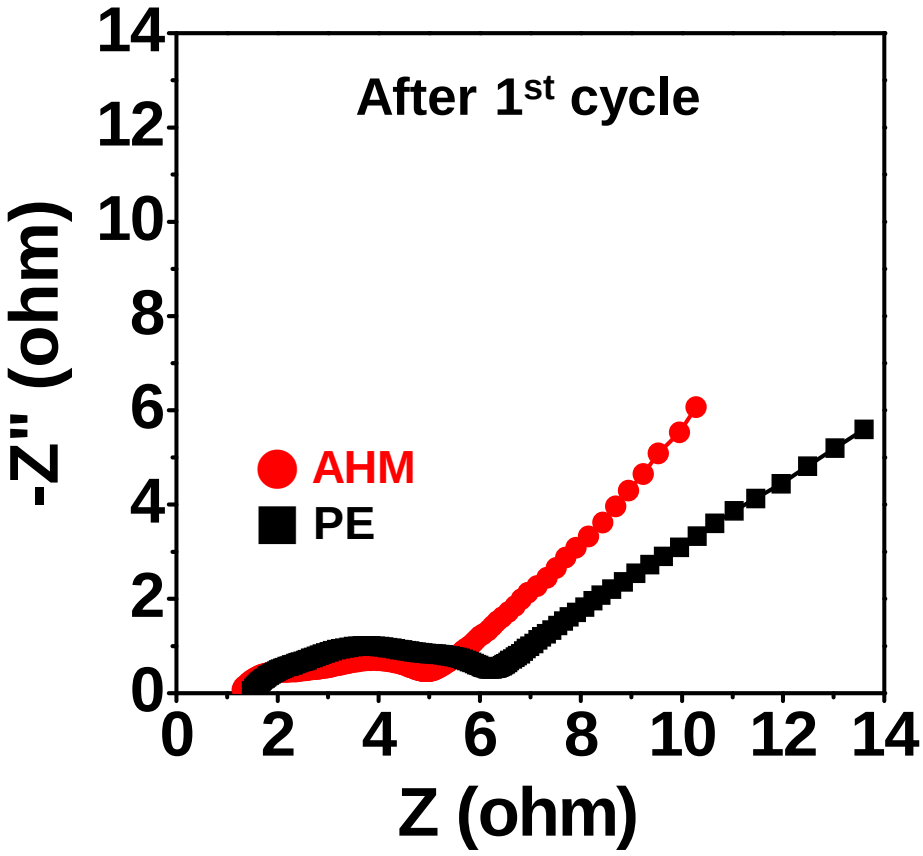

Fig. S9. Comparison in AC impedance spectra after 1st cycle between AHM separator and PE separator.

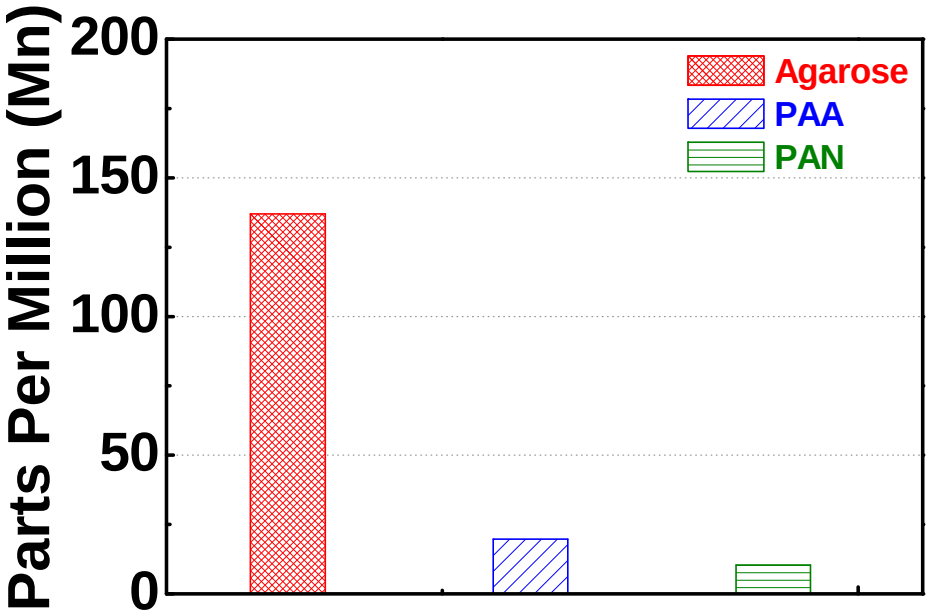

Fig. S10. Quantitative analysis of Mn^{2+} chelation ability of Agarose, PAN and PAA films, where the polymer films were soaked in the $Mn(ClO_4)_2$ solution (10 mM $Mn(ClO_4)_2$-containing 1.3 M $LiPF_6$ in EC/PC = 1/1 v/v) for 2 h at room temperature and then the amount of the captured Mn^{2+} ions was analyzed by ICP-MS measurement.

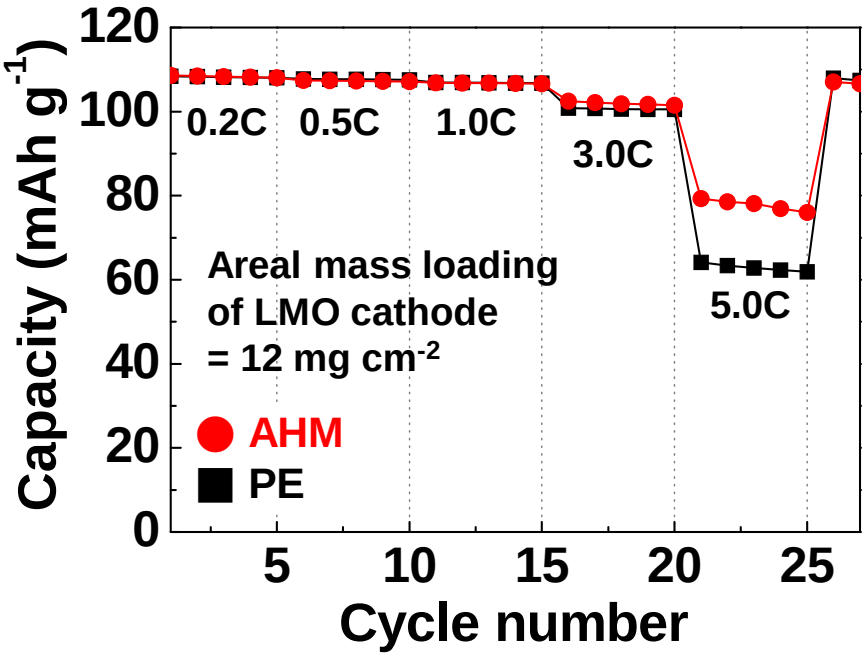

Fig. S11. Discharge rate performance of AHM separator (vs. PE separator) for low mass loading LMO cathode (= 12 mg cm^{-2}).

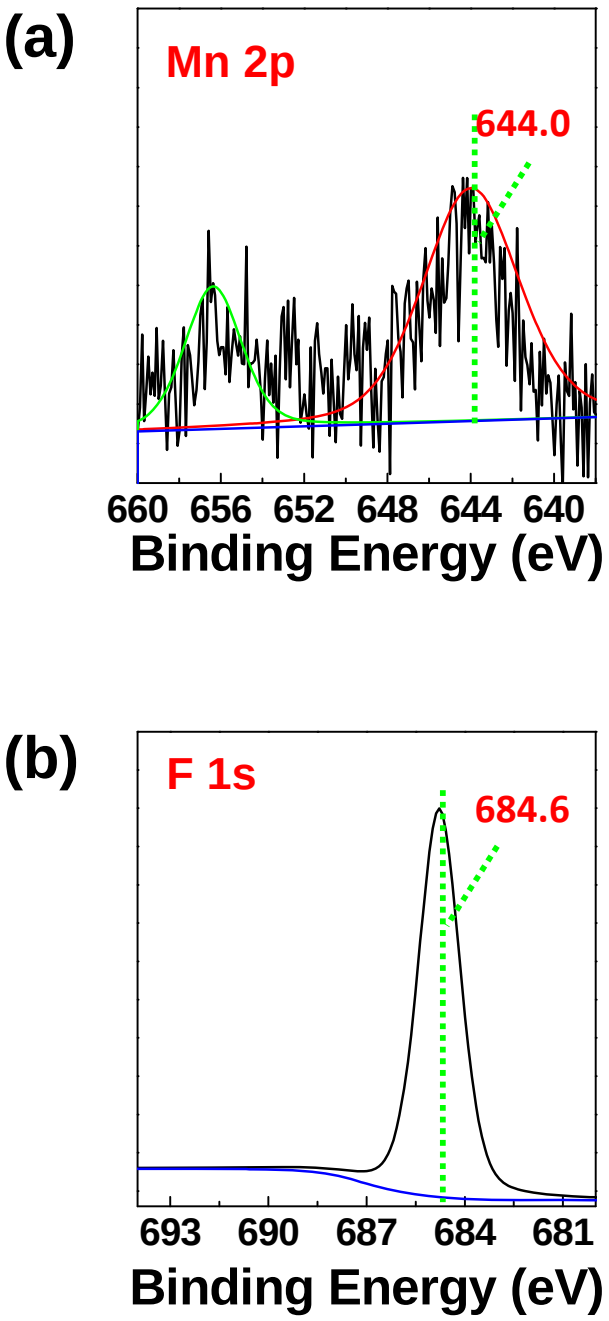

Fig. S12. XPS analysis of AHM separator adjacent to LMO cathode after 100 cycles at 60 ^{o}C: (a) Mn 2p spectra; (b) F 1s spectra.

Table S1. Major membrane properties of AHM separator and PE separator.

	Thickness (mm)	Porosity (%)	Gurley value (sec 100cc^{-1})	Ionic conductivity, σ_S (mS cm^{-1})	MacMullin number, N_M
AHM Separator	25	75	17	0.87	8.68
PE Separator	10	45	240	0.65	11.27

*$N_M = \sigma_o/\sigma_S$
*σ_o = ionic conductivity of liquid electrolyte (1 M $LiPF_6$ in EC/DEC = 1:1 v/v) (= 7.55 mS cm^{-1}).